Applied Medical Informatics
Original Research Vol. 47, No. 3/2025, pp: 85-96

Large Scale Screening of Antibody-Stained Immunohistochemistry Images: An Observational Study on Pancreatic Islets Promotes the Pre-eminence of the ResNet50 Model

Abhijit SAHU[1,2], Sizon NAYAK[2], Pratyush Kumar MAHARANA[2], Pradeep Kumar NAIK[2,*], and Pravash Ranjan MISHRA[1,*]

[1] Department of Anatomy, All India institutes of medical sciences, Bhubaneswar-751019, Odisha, India.
[2] Research Centre of Excellence in Natural Products and Therapeutics, Department of Biotechnology and Bioinformatics, Sambalpur University, Jyoti Vihar, Burla, Sambalpur-768019, Odisha, India.
E-mail(*): pknaik1973@gmail.com (P.K.N.) and mishra.pravash@yahoo.com (P.R.M.)

* Author to whom correspondence should be addressed; Tel.: +91 7894219652

Received: 6 May 2025/Accepted: 26 September 2025/Published online: 27 September 2025

Abstract
Background: The deep neural network (DNN) is a growing field of artificial intelligence that aims to mimic human intelligence. The modern health care system has encouraged this hybrid technology to work smartly and faster to improve efficiency, reduce human error, and support personalized medicine. *Aim*: This article presents an advanced method based on DNN algorithms (ResNet50, EfficientNet, and U-Net) used for the analysis of Immunohistochemistry (IHC) images of pancreatic islets coated with anti-synaptophysin, anti-insulin, and anti-glucagon antibodies. This research aimed to overcome the time-consuming factor, which is a drawn-out process in manual interpretation, and serves as a valuable tool for advancing modern healthcare. *Methods*: The IS-IHC dataset was divided into two groups, training (70%) and test (30%) sets. The models were trained at 500 iterations using a Graphics Processing Unit (GPU) parallel computing architecture and the TensorFlow 2.15 deep learning framework. Several other performance metrics, such as precision, recall, Jaccard, F1 score, and prediction probability, were evaluated to validate the model's accuracy. *Results*: The ResNet50 model automatically detects and quantifies brown-stained regions in IHC images of pancreatic islets, achieving 93.22% accuracy for insulin detection, 90.39% for synaptophysin, and 82.59% for glucagon staining. The model calculates area percentages with precision scores of 93.62% (insulin), 90.33% (synaptophysin), and 89.29% (glucagon), closely matching manual ImageJ calculations, suggesting its superiority over the other two models. The ResNet50 performance was also comparable to manual calculations performed using ImageJ software. Moreover, a high F1 score and prediction probability indicate that the model makes both precise and comprehensive predictions. *Conclusion:* This study found that a ResNet50-based deep learning model enables robust, automated quantification of immunohistochemical markers in pancreatic islets. It achieves high concordance with manual annotation and offering a scalable, objective, and time-efficient computational tool to advance diagnostic accuracy and digital pathology integration in clinical practice.

Keywords: Machine Learning (ML); Deep Neural Network (DNN); Immunohistochemistry (IHC); Pancreatic islet; Diabetes mellitus (DM).

Introduction

Machine learning (ML) techniques play crucial roles in healthcare systems for the early detection of disorders from histopathological images (hematoxylin and eosin (H&E) and IHC) [1-3]. It is described as a machine's ability

to mimic intelligent human behavior based on colour dispersal and staining intensity in tissue sections. The algorithms are trained to learn from the input data and predict the result based on comparable features from the newly imported data [1]. Several ML algorithms have been developed to detect regions of interest from IHC images. Several authors have utilized different machine learning algorithms, such as four deep learning models based on CNNs, recurrent neural networks (RNNs), deep belief networks (DBNs), and autoencoder architectures. However, the other model, i.e., YOLO version 2, which is also based on the CNN architecture, has been reported to achieve high accuracy in detecting region of interest (ROIs) from various IHC and H&E images [4,5]. Both models accurately detect lymphocytes in tissues from breast, colon, prostate, and gastric cancers, as well as other immune cells more precisely, with a good accuracy score [4-6]. The automated algorithms improve efficiency by reducing image analysis time from hours to minutes, reduce human error through standardized quantitative measurements that eliminate subjective visual interpretation, and support personalized medicine by enabling rapid, reproducible biomarker quantification for treatment decision-making**.** The DNN represents an advanced paradigm within diverse machine learning techniques that uses multiple hidden abstraction levels to address pattern recognition issues and extract complex features from the raw data [7]. After the introduction of DNNs in the late 20th century [8], they became more desirable models in healthcare research fields because of their ability to learn complex patterns from large datasets. Their capacity for rapid and accurate prediction from IHC images, along with their effectiveness in biomarker identification, has made them valuable tools in clinical and diagnostic applications [9]. Hinton developed the first DNN, which was based on a unique deep-structured training model called the deep belief network (DBN) [10]. These techniques are beneficial for signal and image processing in breast and lung cancer cases, detecting abnormalities such as tumors, nodules, and other cancerous regions with high accuracy [10]. Additionally, the DNN approach helps in quicker supervision and symbolic information from biological images by learning from hierarchical features (time domain and frequency transformation) than handmade features by training, validation, and test datasets [11]. The most common modules in DNNs are TensorFlow and Keras, which stand out because of their comparatively virtuous accuracy scores compared with those of other neural network models, such as PyTorch and Caffe [12,13]. Building on the high accuracy scores demonstrated by these DNN modules, the present study utilizes the TensorFlow framework to detect ROIs and calculate the area percentage from IHC images of pancreatic islets. IHC remains the gold standard method for detecting proteins of interest in specific cell types. However, a professional technician or pathologist can only interpret this result manually, which takes a long time to validate and is prone to delays in early diagnosis [2]. Therefore, there is a need to develop an automated model that inevitably detects positive regions with good accuracy scores, which would be beneficial for the modern healthcare system.

Diabetes mellitus is a chronic metabolic disorder affecting millions of individuals (approx. 529 million) worldwide [14]. Reports on diabetes revealed that the β-cell mass gradually decreases in individuals with diabetes compared with normal individuals [15]. In our previous study, we detected the total islet area, β-cell area, and α-cell area using the primary antibodies, i.e., anti-synaptophysin, anti-insulin, and anti-glucagon, respectively. Based on the intensity of the above antibodies, the positive area and area percentage of the islet, β- and α-cells were calculated manually using Image J software. However, analyzing these data is time-consuming, and different parameters (such as ROI, hue, and color) must be set manually [15]. To overcome these limitations, our study aimed to developed a deep neural network model using ResNet50, EfficientNet, and U-Net models with four key capabilities i.e., automatic identification of positive (brown) staining regions in pancreatic islet IHC images, calculation of the percentage of positive area for three specific antibodies (synaptophysin, insulin, and glucagon), processing images 10-20 times faster than manual analysis, and achieving accuracy comparable to manual expert analysis (>90% for insulin and synaptophysin). Additionally, a comparative performance analysis was conducted among the three models to determine the most effective approach for automated pancreatic islet quantification. Such an automated model is beneficial for routine diagnostic workflows and digital pathology, which serve as valuable tools for advancing modern healthcare.

Materials and Methods

Collection, Sample Preparation, and Immunostaining

Postmortem pancreatic tissue samples were used for immunohistochemistry. The samples (n=9) were collected from the head, body, and tail regions of the pancreas and stored in 10% neutral buffered formalin, followed by the preparation of paraffin blocks as per our standard laboratory procedure [16]. Hematoxylin and eosin (H&E) staining was performed first to examine the autolytic changes. Tissues with good architecture were further subjected to IHC staining. Immunohistochemistry was performed on three consecutive 4 µM thick paraffin sections with a rabbit monoclonal anti-synaptophysin antibody (Pathnsitu, Livermore, California), a rabbit monoclonal anti-insulin antibody (Pathnsitu, Livermore, California), and a mouse monoclonal anti-glucagon antibody (Bioss Inc., USA) [17]. The primary antibody was detected by a secondary antibody labelled with horseradish peroxidase (HRP) and 3,3'-diaminobenzidine (DAB) chromogen (Pathnitu, Livermore, California). The stained pancreatic islets were captured under a brightfield microscope (Nikon Eclipse Ts2) (Figure 1) [15].

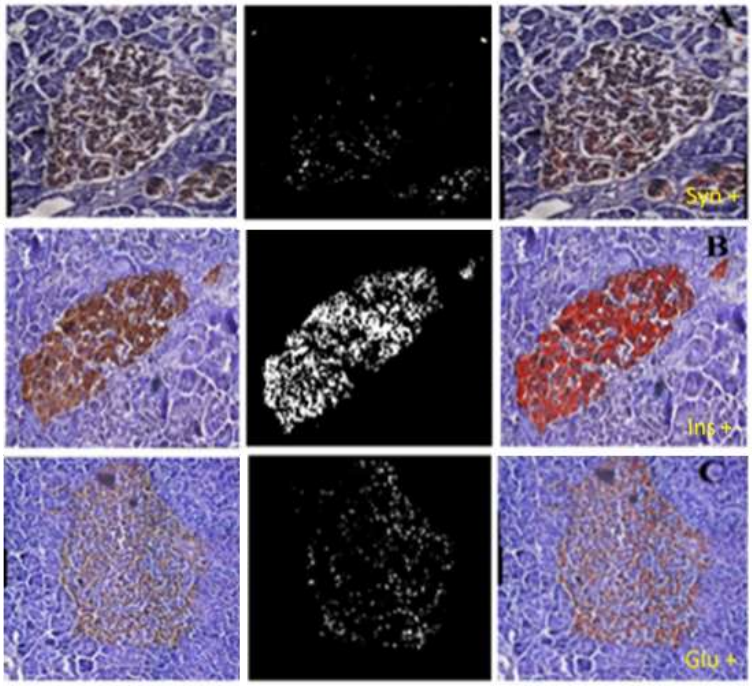

Figure 1. Panel represents the overlay (colored) positive areas of synaptophysin (A), insulin (B), and glucagon (C) from the pancreatic tissue using ResNet50, EfficientNet, and U-Net models.

Dataset

A total of 1300 IHC images of human pancreatic islets were acquired, comprising 433 stained with anti-synaptophysin, 433 with anti-insulin, and 434 with anti-glucagon antibodies. To ensure reproducibility and avoid selection bias, the dataset was divided into training and test sets using stratified random sampling with a fixed random seed (42) within the TensorFlow 2.15 framework. Prior to splitting, all images were randomly shuffled, and stratification was applied to maintain proportional representation of each antibody class across both subsets. The final division consisted of 910 images (70%) allocated to the training set and 390 images (30%) to the test set. Specifically, the training set contained 303 synaptophysin, 303 insulin, and 304 glucagon images, while the test set comprised 130 images for each antibody type. No overlap existed between the two sets to ensure unbiased evaluation. To further validate the appropriateness of this split, the distributions of image quality scores and staining intensity values were compared between the training and test subsets using descriptive statistics and the Kolmogorov–Smirnov test. The absence of significant differences ($p > 0.05$) confirmed that both subsets were statistically comparable, supporting the validity of the adopted sampling methodology.

Model Development

Deep Neural Network machine learning was utilized for image analysis. Initially, the images were imported to the TensorFlow module, followed by the ResNet50, EfficientNet, and U-Net models [18] to enhance visibility and precisely detect the positive regions from the pancreatic islets and calculate the area percentage. ResNet50, renowned for its deep residual learning, effectively mitigates the vanishing gradient problem and offers robust feature extraction in deep networks. In contrast, EfficientNet is acclaimed for its scalability and parameter efficiency, achieving high performance with fewer computational resources. All the models were fine-tuned on the dataset to leverage transfer learning, enhancing their capacity to effectively distinguish the positive area (brown-stained). Initially, images were converted from BGR (Blue-Green-Red) to RGB (Red-Green-Blue) format, a necessary preprocessing step since some image processing libraries load images in BGR order while deep learning models typically expect RGB order to align with standard imaging protocols, ensuring consistent color representation (Figure 1). The hue saturation value (HSV) color space, a crucial marker for stained islet areas, was subsequently employed to detect positive regions. The threshold values for HSV were meticulously tuned, with a lower bound [10, 50, 20] and an upper bound [30, 255, 200], by optimizing the sensitivity and specificity in positive area detection. Morphological operations, including closing (dilation followed by erosion) and opening (erosion followed by dilation), were applied to refine the segmentation by eliminating noise and filling gaps. After HSV, the positive area concerning the positive pixel in the slide was detected and overlay detection was applied for scrupulous differentiation. A performance evaluation was conducted using a comprehensive set of metrics to provide a multidimensional assessment of model efficacy. Several parameters were imported into the model to predict the positive instances and accurately calculate the area percentage.

Training & Validation of the Model

The developed DNN model was trained at 500 iterations using a Graphics Processing Unit (GPU) parallel computing architecture and the TensorFlow 2.15 deep learning framework. Graphics Processing Unit were utilized to accelerate the training process through their ability to perform thousands of parallel computations simultaneously, significantly reducing training time compared to traditional CPU-based processing. The initial learning rate of the model was set to 0.001, approximately 50 epochs. Adam, an optimization algorithm commonly used to adapt the learning rate of each added parameter, was imported into the module for better optimization.

Performance Metrics Analysis

The positive area percentage of the three stained slides was calculated to determine the proportion of positive (brown-stained) pixels. The performances of ResNet50, EfficientNet, and U-Net were evaluated in comparison to manually calculated results obtained using ImageJ. Additionally, the model prediction probability was analyzed to gauge the confidence of the classification output, ensuring reliable segmentation. The key performance metrics included accuracy (ACC) to measure overall correctness(Eq1), precision (PR) to reflect the model's ability to avoid false positives (Eq2), recall (RE) to capture sensitivity towards true positives (Eq3), Jaccard score (JS) to demonstrate the overlap between the predicted positive instances and the actual positive instances (Eq4), and the F1 score (F1) as a harmonic mean of precision and recall for balanced performance evaluation (Eq5). These metrics collectively provided insights into the model's robustness, reliability, and clinical applicability in detecting and quantifying positive regions in islet tissues. The resulting data were imported into an Excel file, and the images were stored.

$$\text{Accuracy (ACC)} = \frac{TP+TN}{TP+FP+TN+TP} \quad (1)$$

$$\text{Precision (PR)} = \frac{TP}{TP+FP} \quad (2)$$

$$\text{Recall (RE)} = \frac{TP}{TP+FN} \quad (3)$$

$$\text{Jaccard score (JC)} = \frac{TP}{TP+FP+FN} \quad (4)$$

$$\text{F1 Score (F1)} = \frac{2 \times Precision \times Recall}{Precision + Recall} \quad (5)$$

where, TP: True Positive (correctly identified positive cases); FP: False Positive (incorrectly identified as positive); FN: False Negative (incorrectly identified as negative); TN: True Negative (correctly identified negative cases).

Results

Immunohistochemical staining using three antibodies (synaptophysin, insulin, and glucagon) demonstrated characteristic brown chromogenic deposits indicating positive immunoreactivity within pancreatic islet cells (Figure 2).

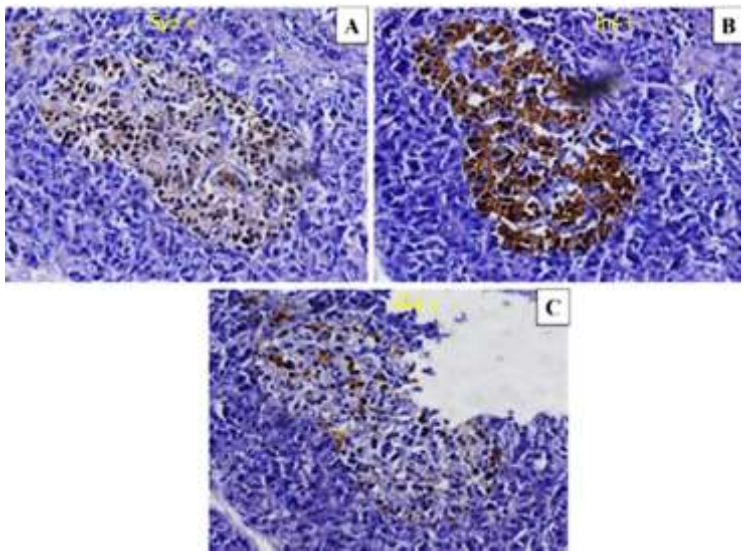

Figure 2. IHC staining of human pancreatic islets. (A) Synaptophysin-positive area, (B) insulin-positive area, and (C) glucagon-positive area. The intensity of the anti-insulin antibody was greater than that of the anti-glucagon and anti-synaptophysin antibodies. Brown area: positive for the respective antibody.

Automated analysis revealed distinct positive staining areas (brown patches) across all images. Area percentage calculations done manually and automated by ResNet50, EfficientNet, and U-Net are presented in Table 1.

Table 1. Area percentage calculation of the three stained antibodies: manually, with Resnet50, EfficientNet and U-Net.

No	Stained Group	Area percentage
Manual calculation		
1	SYN	96.05 ± 2.06
2	INS	58.12 ± 8.30
3	GLU	23.09 ± 7.32
Automated calculation using Resnet50		
1	SYN	94.13 ± 1.03
2	INS	51.43 ± 2.14
3	GLU	21.09 ± 5.64
Automated calculation using EfficientNet		
1	SYN	82.41 ± 3.09
2	INS	47.05 ± 3.78
3	GLU	19.01 ± 1.46
Automated calculation using U-Net		
1	SYN	74.12 ± 1.43
2	INS	44.45 ± 2.07

3	GLU	14.19 ± 3.36

SYN-Synaptophysin, INS-insulin, GLU-glucagon.

Figures 3, 4, and 5 present the prediction results of the positive area of pancreatic islets using the ResNet50, EfficientNet, and U-Net models, respectively. These comparative results revealed the performance of ResNet50 compared to EfficientNet and U-Net across various performance metrics, including prediction probability. ResNet50 achieved a higher prediction probability score for automatic detection and calculation of the positive area.

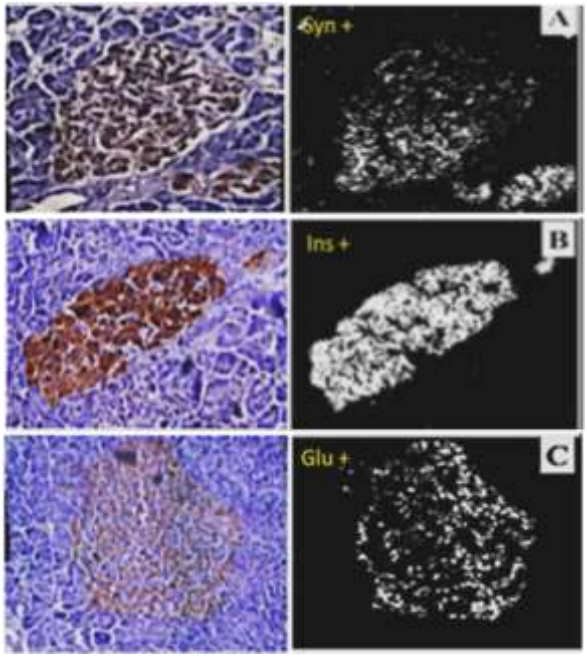

Figure 3. Panel representing the prediction of positive areas from whole pancreas sections from the ResNet50 model. The left image shows the positive areas of synaptophysin (A), insulin (B), and glucagon (C), and the right-side images show the prediction of the positive area.

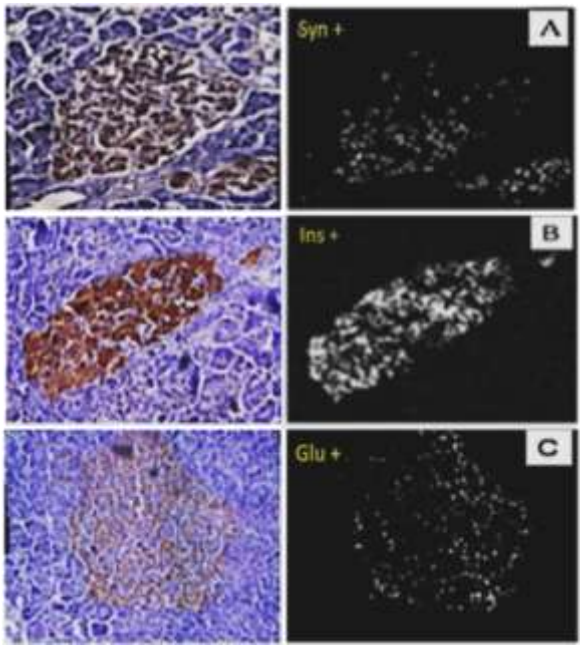

Figure 4. Panel illustrating the predictions of positive images generated by the EfficientNet model. The left image shows the positive areas of synaptophysin (A), insulin (B), and glucagon (C), and the right-side images show the prediction of the positive area.

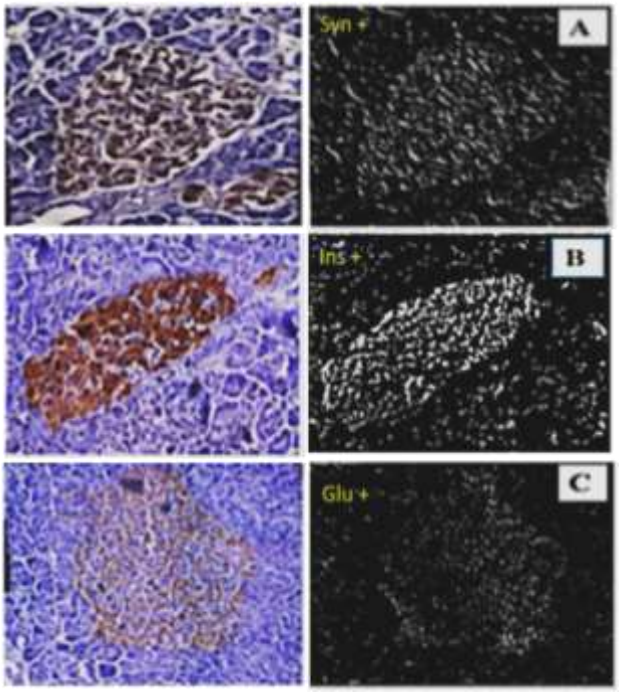

Figure 5. Panel representing the prediction of positive images from the U-Net model. The left image shows the positive areas of synaptophysin (A), insulin (B), and glucagon (C), and the right-side images show the prediction of the positive area.

Performance Scoring of the Models

The prediction results of all three stained images were promising, with an average accuracy around 93%. The ResNet50 model accurately predicted and calculated the positive area percentage of pancreatic islets compared to the other models (Table 2).

Table 2. Performance metric scores of the three models.

Stained slides	Precision (%)	Recall Percentage (%)	Jaccard score (%)	F1 score (%)	Predictive probability (%)	Accuracy (%)
ResNet50						
SYN	90.33	89.47	88.19	89.06	90.39	90.39
INS	93.62	88.94	85.66	90.21	93.22	93.22
GLU	89.29	96.89	79.96	80.65	82.59	82.59
EfficientNet						
SYN	61	62.70	59.92	62.09	48.40	70.76
INS	89	73.95	78.02	79.67	65.29	80.85
GLU	64.19	67.33	58.65	58.09	46.40	69.32
U-Net						
SYN	84	82.65	84.89	87	70.21	85.03
INS	81	80.29	80.60	82	62.89	81.45
GLU	78.21	78.03	78.05	72	61.09	75.56

SYN = synaptophysin, INS = insulin, GLU = glucagon-stained islets,

ResNet50 model demonstrated superior performance across all evaluation metrics since outperform both the models i.e., EfficientNet and U-Net. Precision scores were similarly and area percentage calculations by ResNet50 showed the closest agreement with manual ImageJ calculation among the three models tested (Table 1).

Discussion

Our study demonstrated that the DNN models developed by different machine learning approaches (such as ResNet50, EfficientNet and U-Net) precisely detect the positive area of the pancreatic islets and calculate its area percentage, which is comparable with the manually calculated data. A comparative analysis of the different models (ResNet50, EfficientNet, and U-Net) revealed that a higher prediction accuracy score and confidence in identifying positive areas were obtained from the ResNet50 model (Table 2). This superior performance is because the residual connections in ResNet50 likely contribute to better feature extraction (complex textures and subtle staining patterns require robust hierarchical representation) than others do, especially in IHC images with complex textures [19]. Similarly, Chen *et al.* (2013) reported that the CNN algorithm was employed to develop pancreas ++ software that is able to segment pancreatic structures (differentiate α & β-cells) from fluorescence images of pancreatic islets [20].

The high accuracy and strong correlation of our ResNet50 model compared with the manual quantification highlights its potential for integration into real-world diagnostic and research settings. In clinical pathology, manual IHC scoring is not only time-consuming but also subject to inter-observer variability, which can impact diagnostic consistency and treatment decisions. Our model offers an automated, standardized, and reproducible alternative that can generate quantitative results in seconds, significantly accelerating turnaround time without sacrificing precision. This capability is particularly valuable in high-volume labs, multi-centric studies, or resource limited settings where expert pathologist time is constrained. Moreover, the model's adaptability with appropriate retraining to other. IHC markers or tissue types including breast, prostate, thyroid positions it as a scalable tool for expanding AI-assisted pathology beyond pancreatic islets. By reducing human workload and minimizing subjective bias, this approach helps to move pathology towards precision diagnostics. Here, AI-enhanced quantitative analysis complements not only replaces expert interpretation but leads to greater diagnostic confidence, improved workflow efficiency, and better patient care pathways.

The advancement of machine learning over the last decade has revolutionized the debate around digital pathology and opened up prospects for better diagnosis through computational pathology [21]. Traditionally, pathologists analyse histological samples by applying H&E or performing IHC using molecular markers and examining them manually under a light microscope [13]. This examination helps them in diagnosis by highlighting specific cellular components, enabling accurate diagnosis and classification of diseases; in addition, it also plays a role in predicting therapeutic response and guiding personalized treatment strategies [22]. The traditional manual evaluations are time-consuming and may delay scheduling of treatment strategies [23]. Modern AI technology contributes several machine learning models that automatically detect ROIs from histopathological images within a limited time and obtain reasonable scores to overcome time constraints [24].

In the modern healthcare system, various newly developed omics technologies, such as genomics, transcriptomics, and proteomics, play crucial roles in better understanding molecular processes [13]. In terms of automated scoring of the IHC images, several commercial software packages offering quantitative image analysis were developed, i.e., ACIS (ChromaVision Medical Systems, Inc., San Juan Capistrano, CA, USA), Ariol SL-50 (Applied Imaging, San Jose, CA, USA), iVision and GenoMx (BioGenex, San Ramon, CA, USA), AQUA (HistoRx, New Haven, CT, USA), LSC Laser Scanning Cytometer (CompuCyte, Cambridge, MA, USA), BLISS and IHC score (Bacus Laboratories, Inc., Lombard, IL, USA), ScanScope (Aperio Technologies, Inc., Vista, CA, USA), SlidePath's Tissue Image Analysis (Leica Biosystems, Wetzlar, Germany) and Virtuoso (Ventana Medical Systems, Tucson, AZ, USA). The existing commercial software applications have exhibited more repeatable and consistent findings than manual assessment does, and they have been approved for diagnostic usage by the FDA (US Food and Drug Administration) and CE-Mark [25]. However, commercial software implements traditional image processing techniques such as hue, saturation, and brightness, and some even require a pathologist to set thresholds manually before processing [26]. Additionally, several more protruding deep learning algorithms, such as DenseNet and Xception, VGG16, CNNs, and U-Net, have been utilized to recognize segment-specific cells, such as epithelial and stromal cells, benign and malignant cells, immune cells, mitotic cells [27,28] HER2-positive tumor cells in breast cancer [29], Ki67-positive proliferative cells [30,31] and endothelial cell distribution patterns in active and passive smokers from IHC images [32]. As these approaches require manual feature engineering (identifying the ROI from the raw image), they are less effective for immediate image quantification; hence, research in this field

has moved toward DNNs, an advanced branch of machine learning. The DNN learns from raw input to output without extensive preprocessing, allowing the model to learn directly from the raw data [33]. Health Equity Assessment of Machine Learning performance (HEAL), an automated deep learning-based framework, was developed by Wang and team members and is the first software package that combines 16 different deep learning modules into an improved architecture. It includes tools for image preprocessing, hyperparameter optimization (i.e., controlling the training process of the model, including the learning rate, batch size, number of layers or neurons, and dropout rate), model performance evaluation (model accuracy, precision, recall, confusion matrix), and visualization analysis. It has an accuracy score of 97.5% to 99.3% [34]. Hamida and colleagues reported that they classified and quantified the color of the tumor region using the U-Net & S_{EG}NET module of the DNN, with accuracy scores of 76.18% and 81.22%, respectively [35].

Recent reports suggest that HALO, an ML algorithm, accurately annotates the tissue area in a WSI image, the endocrine region, the acinar region, and the ductal area of the pancreatic islet in type 1 diabetic patients [36]. Guo and team developed a deep learning network based on an archetypal analysis network (AA-net), which precisely segments the scattered islets in the pancreas-stained section and identifies the status of the pancreatic islets in the rodent pancreas [37]. This result was similar to the current finding that the present DNN models precisely detect the positive area from the tissue sections and calculate the area percentage, which is comparable with the manually calculated data (Figure 3,4,5). The ResNet50 model detected the ROI and calculated its area percentage more precisely than did the EfficientNet and U-Net models (Table 1). The prediction accuracy score was also greater in this model than in other models, indicating that this approach would be appropriate for analyzing hormone-secreting cells in pancreatic islets and could potentially be adapted for other IHC applications such as carcinoma analysis, lymphocyte identification, differential protein expression, and tumor microenvironment analysis.

Previous studies on the DNN model revealed that to support the accuracy score of the model, several other performance metrics have been employed, i.e., the F1 score, Jaccard index, and recall percentage, which validate the model on the basis of the true positive instances from the images [38]. Hence, here, we have added few performance metrics to validate our model, such as precision, the recall percentage, the Jaccard index, the F1 score, and the prediction probability. These performance metrics also exhibited a comparatively higher score in the ResNet50. The demonstrated performance of this ResNet50-based approach suggests several potential applications in pancreatic islet research. The model could facilitate automated quantification of hormone-secreting cells, potentially reducing analysis time in diabetes research workflows compared to manual ImageJ processing. With further validation, this approach might contribute to standardizing quantitative analysis methods across research laboratories and could potentially be adapted for other hormone-expressing tissue analyses, though such applications would require additional training and validation with tissue-specific datasets. Several limitations should be acknowledged in this study. First, the dataset was derived from a limited sample size of nine postmortem pancreatic tissue specimens, which may not fully represent the diversity of pancreatic islet morphology across different populations, age groups, or pathological conditions. Second, the model was trained and validated exclusively on images obtained using DAB chromogen staining with specific antibodies (synaptophysin, insulin, and glucagon), limiting its applicability to other staining protocols, chromogen systems, or antibody combinations commonly used in different laboratories. Third, the study focused solely on pancreatic islet tissue from postmortem specimens, and the model's performance on other endocrine tissues, live tissue biopsies, or pathological specimens with varying degrees of autolysis remains untested. The reported performance results suggest that machine learning approaches for early detection may be beneficial for the early diagnosis of patients and improved treatment strategies [39].

Conclusion

Our results demonstrated the superiority of ResNet50 over EfficientNet and U-Net for detecting ROIs in IHC images coated with different antibodies. The higher accuracy and performance metrics (precision, recall, and F1 score) validate ResNet50's potential for clinical use in histopathological analysis. These DNN models accurately detect the ROI from new IHC images from different cases, achieving a good predictive accuracy score. The predicted scores were comparable with the manually calculated data. The ResNet50 model's prediction accuracy is sufficient to predict ROIs from new images from different types of new IHC images. The average predictive

accuracy score of our model (ResNet50) for the three image classes ranged from 86% to 91%. In conclusion, computer-aided diagnosis of histopathological IHC images can assist clinicians in diagnosing, classifying, and grading diseases on the basis of severity, allowing for appropriate therapeutic measures in areas without experienced histopathologists. Further research could explore ensemble models or fine-tuning for improved performance.

List of Abbreviations: IHC: Immunohistochemistry, DNN: Deep Neural Network, ML: Machine Learning, SYN: Synaptophysin, INS: Insulin, GLU: Glucagon, ROI: Region Of Interest, CNN: Convolutional Neural Network, HSV: Hue saturation value.

Author Contributions: A.S.: Conceptualization of the work, data acquisition, analysis, methodology, drafting of the Manuscript; S.N.: methodology design, programming, acquisition; P.K.M.: programming, acquisition, drafting of the manuscript, P.K.N.: Conceptualization of the work, critical review of the manuscript for important intellectual content; P.R, M.: Conceptualization of the work, critical review of the manuscript for important intellectual content.

Funding: This research received no funding.

Ethics Statement: The Institute Ethical clearance was obtained from the All India Institute of Medical Sciences, Bhubaneswar Vide approval number: **T/EMF/Anatomy/19/31.**

Data Availability Statement: Data underlying this study's findings can be obtained from the corresponding author.

Acknowledgments: This work has received support from the Indian Council of Medical Research (ICMR) Adhoc Project ID: 2020-0852. We are happy to acknowledge the Centre of Excellence in Natural Products and Therapeutics (COE NPT), Department of Biotechnology & Bioinformatics, Sambalpur University, for providing us with a high-performance computing infrastructure for the smooth execution of the study.

Conflict of Interest: The authors declare that they have no conflicts of interest.

References

1. Alanazi A. Using machine learning for healthcare challenges and opportunities. Inform Med Unlocked 2022;30:2352-9148. https://doi.org/10.1016/j.imu.2022.100924.
2. Shamai G, Binenbaum Y, Slossberg R, Duek I, Gil Z, Kimmel R. Artificial Intelligence Algorithms to Assess Hormonal Status From Tissue Microarrays in Patients with Breast Cancer. JAMA Netw Open 2019;2:e197700. https://doi.org/10.1001/jamanetworkopen.2019.7700.
3. Maharana PK, Behera TK, Naik PK. Machine Learning-Based Classification and Statistical Analysis of Liver Cancer: A Comprehensive Study of Model Performance and Clinical Significance. Appl Med Inform 2024;46:119-128.
4. Garcia E, Hermoza R, Castanon CB, Cano L, Castillo M, Castanñeda C. Automatic Lymphocyte Detection on Gastric Cancer IHC Images Using Deep Learning. Proc IEEE Symp Comput Based Med Syst 2017, pp. 200-204. https://doi.org/10.1001/10.1109/CBMS.2017.94.
5. Rijthoven M van, Swiderska-Chadaj Z, Seeliger K, van der Laak J, Ciompiet F. You Only Look on Lymphocytes Once [Internet] [accessed on 27 March 2025]. Available from: https://openreview.net/forum?id=S10IfW2oz
6. Swiderska-Chadaj Z, Pinckaers H, van Rijthoven M, Balkenhol M, Melnikova M, Geessink O, et al. Learning to detect lymphocytes in immunohistochemistry with deep learning. Med Image Anal 2019;58:101547. https://doi.org/10.1016/j.media.2019.101547.
7. Chakraborty C, Bhattacharya M, Pal S, Lee SS. From machine learning to deep learning: Advances of the recent data-driven paradigm shift in medicine and healthcare. Curr Res Biotechnol 2024;7:100164. https://doi.org/10.1016/j.crbiot.2023.100164.
8. Bengio Y. Learning Deep Architectures for AI. Foundations and Trends® in Machine Learning 2009;2:1-127. https://doi.org/10.1561/2200000006.
9. Jiang X, Hu Z, Wang S, Zhang Y. Deep Learning for Medical Image-Based Cancer Diagnosis. Cancers (Basel) 2023;15:3608. https://doi.org/10.3390/cancers15143608

10. Hinton GE, Osindero S, Teh Y-W. A Fast Learning Algorithm for Deep Belief Nets. Neural Comput. 2006;18: 1527–1554. https://doi.org/10.1162/neco.2006.18.7.1527.
11. Zou K, Wang S, Wang Z, Zhang Z, Yang F. HAR_Locator: a novel protein subcellular location prediction model of immunohistochemistry images based on hybrid attention modules and residual units. Front Mol Biosci. 2023;10:1171429. https://doi.org/10.3389/fmolb.2023.1171429.
12. Smith B, Hermsen M, Lesser E, Ravichandar D, Kremers W. Developing image analysis pipelines of whole-slide images: Pre- and post-processing. J Clin Transl Sci. 2020;5(1):e38. https://doi.org/10.1017/cts.2020.531.
13. Ghoshal B, Hikmet F, Pineau C, Tucker A, Lindskog C. DeepHistoClass: A Novel Strategy for Confident Classification of Immunohistochemistry Images Using Deep Learning. Mol Cell Proteomics. 2021;20:100140. https://doi.org/10.1016/j.mcpro.2021.100140.
14. GBD 2021 Diabetes Collaborators. Global, regional, and national burden of diabetes from 1990 to 2021, with projections of prevalence to 2050: a systematic analysis for the Global Burden of Disease Study 2021. Lancet 2023;402:203–234. https://doi.org/10.1016/ S0140-6736(23)01301-6.
15. Mishra P, Sahu A, Naik PK, Ravi PK. Islet Dimensions and Its Impact on the Cellular Composition and Insulin-Secreting Capacity: Insights Into the Role of Non-beta Cells. Cureus. 2024;16(1):e52428. https://doi.org/10.7759/cureus.52428.
16. Ravi PK, Purkait S, Singh SR, Mishra PR. Decay score: a guide to the immunoreactivity of human pancreatic islets in autopsy specimen. Folia Morphol (Warsz). 2022;81(1):101-106. https://doi.org/10.5603/FM.a2021.0002.
17. Sahu A, Mishra PR, Pragyandipta P, Rath S, Nanda A, Kanhar S, et al. Elucidating the therapeutic efficacy of polyherbal formulation for the management of diabetes through endogenous pancreatic β-cell regeneration. Bioorg Chem. 2025;157:108270. https://doi.org/10.1016/j.bioorg.2025.108270.
18. Kansal K, Chandra TB, Singh A. ResNet-50 vs. EfficientNet-B0: Multi-Centric Classification of Various Lung Abnormalities Using Deep Learning. Procedia Comput Sci. 2024;235:70-80. https://doi.org/10.1016/j.procs.2024.04.007.
19. Jiang B, Bao L, He S, Chen X, Jin Z, Ye Y. Deep learning applications in breast cancer histopathological imaging: diagnosis, treatment, and prognosis. Breast Cancer Res. 2024;26(1):137. https://doi.org/10.1186/s13058-024-01895-6.
20. Chen H, Martin B, Cai H, Fiori JL, Egan JM, Siddiqui S, Maudsley S. Pancreas++: automated quantification of pancreatic islet cells in microscopy images. Front Physiol. 2013;3:482. https://doi.org/10.3389/fphys.2012.00482.
21. Smith B, Hermsen M, Lesser E, Ravichandar D, Kremers W. Developing image analysis pipelines of whole-slide images: Pre- and post-processing. J Clin Transl Sci. 2020;5(1):e38. https://doi.org/10.1017/cts.2020.531.
22. Morrison LE, Lefever MR, Lewis HN, Kapadia MJ, Bauer DR. Conventional histological and cytological staining with simultaneous immunohistochemistry enabled by invisible chromogens. Lab Invest. 2022;102(5):545-553. https://doi.org/10.1038/s41374-021-00714-2.
23. Wasinger G, Koeller MC, Compérat E. Pathology in the artificial intelligence era: practical insights for immunohistochemistry and molecular pathology. Diagn Histopathol. 2025;31(7):416-423. https://doi.org/10.1016/J.MPDHP.2025.04.003.
24. Homeyer A, Geißler C, Schwen LO, Zakrzewski F, Evans T, Strohmenger K, et al. Recommendations on compiling test datasets for evaluating artificial intelligence solutions in pathology. Mod Pathol. 2022;35(12):1759-1769. https://doi.org/ 10.1038/s41379-022-01147-y. Erratum in: Mod Pathol. 2022;35(12):2034. https://doi.org/10.1038/s41379-022-01163-y.
25. García-Rojo M, De Mena D, Muriel-Cueto P, Atienza-Cuevas L, Domínguez-Gómez M, Bueno G. New European Union Regulations Related to Whole Slide Image Scanners and Image Analysis Software. J Pathol Inform. 2019;10:2. https://doi.org/10.4103/jpi.jpi_33_18.
26. Priego-Torres BM, Lobato-Delgado B, Atienza-Cuevas L, Sanchez-Morillo D. Deep learning-based instance segmentation for the precise automated quantification of digital breast cancer immunohistochemistry images. Expert Syst Appl. 2022;193:116471. https://doi.org/10.1016/j.eswa.2021.116471.

27. Swiderska-Chadaj Z, Pinckaers H, van Rijthoven M, Balkenhol M, Melnikova M, Geessink O, et al. Learning to detect lymphocytes in immunohistochemistry with deep learning. Med Image Anal. 2019;58:101547. https://doi.org/10.1016/j.media.2019.101547.
28. Aprupe L, Litjens G, Brinker TJ, van der Laak J, Grabe N. Robust and accurate quantification of biomarkers of immune cells in lung cancer micro-environment using deep convolutional neural networks. PeerJ. 2019;7:e6335. https://doi.org/10.7717/peerj.6335.
29. Tewary S, Arun I, Ahmed R, Chatterjee S, Mukhopadhyay S. AutoIHC-Analyzer: computer-assisted microscopy for automated membrane extraction/scoring in HER2 molecular markers. J Microsc. 2021;281(1):87-96. https://doi.org/10.1111/jmi.12955.
30. Feng M, Deng Y, Yang L, Jing Q, Zhang Z, Xu L, et al. Automated quantitative analysis of Ki-67 staining and HE images recognition and registration based on whole tissue sections in breast carcinoma. Diagn Pathol. 2020;15(1):65. https://doi.org/10.1186/s13000-020-00957-5.
31. Saha M, Chakraborty C, Arun I, Ahmed R, Chatterjee S. An Advanced Deep Learning Approach for Ki-67 Stained Hotspot Detection and Proliferation Rate Scoring for Prognostic Evaluation of Breast Cancer. Sci Rep. 2017;7:3213. https://doi.org/10.1038/s41598-017-03405-5
32. Bastia B, Kumar K, Kumar SN, Behera NR, Jain AK. Expression of Endothelin-1 in Human Placenta of Active Smokers: An Immunohistochemical Study. Int J Res Stud Biosci. 2017;5(12):34-40. https://doi.org/10.20431/2349-0365.0512005.
33. Tran KA, Kondrashova O, Bradley A, Williams ED, Pearson JV, Waddell N. Deep learning in cancer diagnosis, prognosis and treatment selection. Genome Med. 2021;13(1):152. https://doi.org/10.1186/s13073-021-00968-x.
34. Wang Y, Coudray N, Zhao Y, Li F, Hu C, Zhang YZ, et al. HEAL: an automated deep learning framework for cancer histopathology image analysis. Bioinformatics. 2021;37(22):4291-4295. https://doi.org/10.1093/bioinformatics/btab380.
35. Ben Hamida A, Devanne M, Weber J, Truntzer C, Derangère V, Ghiringhelli F, et al. Deep learning for colon cancer histopathological images analysis. Comput Biol Med. 2021;136:104730. https://doi.org/10.1016/j.compbiomed.2021.104730.
36. Tang X, Kusmartseva I, Kulkarni S, Posgai A, Speier S, Schatz DA, et al. Image-Based Machine Learning Algorithms for Disease Characterization in the Human Type 1 Diabetes Pancreas. Am J Pathol. 2021;191(3):454-462. https://doi.org/10.1016/j.ajpath.2020.11.010.
37. Guo Q, AlKendi A, Jiang X, Mittone A, Wang L, Larsson E, et al. Reduced volume of diabetic pancreatic islets in rodents detected by synchrotron X-ray phase-contrast microtomography and deep learning network. Heliyon. 2023;9(2):e13081. https://doi.org/10.1016/j.heliyon.2023.e13081.
38. Klimov S, Xue Y, Gertych A, Graham RP, Jiang Y, Bhattarai S, et al. Predicting Metastasis Risk in Pancreatic Neuroendocrine Tumors Using Deep Learning Image Analysis. Front Oncol. 2021;10:593211. https://doi.org/10.3389/fonc.2020.593211.
39. Couture HD, Williams LA, Geradts J, Nyante SJ, Butler EN, Marron JS, et al. Image analysis with deep learning to predict breast cancer grade, ER status, histologic subtype, and intrinsic subtype. npj Breast Cancer 2018;4:30. https://doi.org/10.1038/s41523-018-0079-1